

Shear Power Spectrum Reconstruction using Pseudo-Spectrum Method

Chiaki Hikage¹, Masahiro Takada², Takashi Hamana³, David Spergel^{1,2}

¹ *Department of Astrophysical Sciences, Princeton University, Peyton Hall, Princeton NJ 08544, USA*

² *Institute for the Physics and Mathematics of the Universe (IPMU), The University of Tokyo, Chiba 277-8582, Japan*

³ *National Astronomical Observatory of Japan, Tokyo 181-8588, Japan*

23 October 2018

ABSTRACT

We develop a pseudo power spectrum technique for measuring the lensing power spectrum from weak lensing surveys in both the full sky and flat sky limits. The power spectrum approaches have a number of advantages over the traditional correlation function approach. We test the pseudo spectrum method by using numerical simulations with square-shape boundary that include masked regions with complex configuration due to bright stars and saturated spikes. Even when 25% of total area of the survey is masked, the method recovers the E -mode power spectrum at a sub-percent precision over a wide range of multipoles $100 \lesssim \ell \lesssim 10^4$. The systematic error is smaller than the statistical errors expected for a 2000 square degree survey. The residual B -mode spectrum is well suppressed in the amplitudes at less than a percent level relative to the E -mode. We also find that the correlated errors of binned power spectra caused by the survey geometry effects are not significant. Our method is applicable to the current and upcoming wide-field lensing surveys.

Key words: cosmology: theory — gravitational lensing — large-scale structure of universe

1 INTRODUCTION

Large scale structure deflects light rays as they propagate from distant galaxies to us, thus distorting the shapes of these galaxies (e.g., Bartelmann & Schneider 2001; Hoekstra & Jain 2008, for thorough reviews). This weak lensing or cosmic shear signals measures a combination of the total matter distribution projected along the line-of-sight and the angular diameter distance. Since the first measurements of weak lensing only a decade ago (Van Waerbeke et al. 2000; Wittman et al. 2000; Bacon, Refregier & Ellis 2000; Kaiser, Wilson & Luppino 2000), there have been major improvements as surveys continue to grow in size and depth (e.g. Fu et al. 2008; Ichiki, Takada & Takahashi 2009; Schrabback et al. 2010, for the latest results). Gravitational lensing is one of the most promising methods of constraining cosmology including the nature of dark energy (e.g. Takada & Bridle 2007). There are various on-going and planned surveys aimed at studying dark energy through the high-precision weak lensing measurements: the CFHT Legacy Survey¹, the Hyper Suprime-Cam Weak Lensing Survey (Miyazaki et al. 2006),

the Dark Energy Survey (DES)², and ultimately Large Synoptic Survey Telescope (LSST)³, Euclid (Refregier et al. 2010), and Joint Dark Energy Mission (JDEM).

How should we analyze these new lensing data set? Most researchers use the two-point correlation function to characterize the cosmic shear signals. The correlation function method can be easily applied to complex survey geometries involving partial sky coverage and masked regions. However, the errors in the measurement are highly correlated between different bins (see Schneider et al. 2002; Joachimi, Schneider & Efler 2008, for the detailed studies). Even if the shear field follows Gaussian statistics, which is a good approximation in the linear regime, there are large correlations between different angular-scale bins. These correlations are even larger, and more model-dependent on the smaller scales that contain most of the current observational information. Since the accurate estimate of the covariances is essential for robust cosmological constraints, a large number of numerical simulations are necessary (Semboloni et al. 2007).

The power spectrum, the Fourier- or Harmonic-transformed counterpart of the two-point correlation func-

¹ <http://www.cfht.hawaii.edu/Science/CFHLS/>

² <http://www.darkenergysurvey.org>

³ <http://www.lsst.org>

tion, is an alternative means of measuring the cosmic shear correlations. Whilst the correlation function and power spectrum are mathematically equivalent, the power spectrum measurement of cosmic shear has been used less (see the COMBO 17-survey by Brown et al. 2003). The power spectrum approach has a number of advantages: its theoretical interpretation is simpler and there are weaker correlations between band powers at different multipoles. For example, the different bins are independent for the Gaussian field or on large angular scales. Even for small angular scales affected by nonlinear structure formation, the power spectrum covariances are relatively well understood through both analytical models and simulations of nonlinear structure formation (Hu & White 2001; Cooray & Hu 2001; Takada & Jain 2009; Sato et al. 2009; Pielorz et al. 2009). The disadvantage is the presence of finite sky coverage and masked regions, which breaks the orthogonality of Fourier/Harmonic components. One needs to properly deal with the survey geometry effect to estimate unbiased power spectrum.

The purpose of this paper is to eliminate this disadvantage. We employ the *pseudo* power spectrum technique, which is well developed in the CMB studies (e.g. Wandelt, Hivon & Gorski 2001)⁴. For the first time, we apply the method to recover the lensing power spectrum from the shear field taking into account incomplete survey geometry. To assess the performance of this method, we make simulated shear maps including a realistic configuration of masked regions due to bright stars and saturated spikes. Furthermore, we develop the method for both the full-sky and flat-sky approaches. The full-sky approach is adequate for reconstructing large angular-scale modes that are relevant for the curvature of the sky. On the other hand, the flat-sky approach should serve as a practically useful approximation of sub-degree scale modes, which carry most of useful cosmological information in the shear power spectrum. We find that the pseudo power spectrum method allows for an unbiased estimate of the underlying *E*-mode power spectrum over a range of angular scales we study. We also show that the residual *B*-mode power spectrum, which is leaked from *E*-mode power due to an imperfect reconstruction, can be well suppressed. Our method can be applied to the existing data and forthcoming weak lensing surveys.

The paper is organized as follows: Section 2 describes the pseudo spectrum method to deconvolve shear power spectra with inhomogeneous survey mask. Section 3 describes the simulation maps we use to test the deconvolution method. We employ two different simulation maps: one is Gaussian shear maps and the other is the ray-tracing simulations of shear maps including the non-Gaussian effects due to nonlinear structure formation. Section 4 shows the results of both the full-sky and flat-sky approaches. Section 5 is devoted to the summary and conclusions.

2 METHODOLOGY: RECONSTRUCTION OF SHEAR POWER SPECTRUM

In this section we briefly review a method for reconstructing shear power spectra from the pseudo-spectrum estimators.

⁴ See Seljak (1998) and Hu & White (2001) for the maximum likelihood method of shear power spectrum estimation.

We take into account an imperfect survey geometry due to survey boundary and masking effect. The method is analogous to the one used in estimating CMB polarization power spectra (Kogut et al. 2003; Brown, Castro & Taylor 2005).

2.1 Full Sky Formalism

Since the shear field is a spin-2 field, the *E*- and *B*-mode harmonic coefficients of the shear fields γ_i ($i = 1, 2$) can be expressed in the spherical harmonic expansion as

$$E_{lm} \pm iB_{lm} = \oint d\Omega_{\hat{\mathbf{n}}} [\gamma_1(\hat{\mathbf{n}}) \pm i\gamma_2(\hat{\mathbf{n}})]_{\pm 2} Y_{lm}^*(\hat{\mathbf{n}}), \quad (1)$$

and the inverse relation is

$$\gamma_1(\hat{\mathbf{n}}) \pm i\gamma_2(\hat{\mathbf{n}}) = \sum_{lm} [E_{lm} \pm iB_{lm}]_{\pm 2} Y_{lm}(\hat{\mathbf{n}}), \quad (2)$$

where $_{\pm 2}Y_{lm}$ is the spin-2 spherical harmonics, and $\hat{\mathbf{n}}$ denotes the unit vector specifying the angular direction on the sky. The integration range is over the full sky.

In the linear regime, the statistical information in the map is fully encoded in the power spectra

$$C_l^{EE} \equiv \frac{1}{2l+1} \sum_m |E_{lm}|^2, \quad (3)$$

$$C_l^{BB} \equiv \frac{1}{2l+1} \sum_m |B_{lm}|^2, \quad (4)$$

$$C_l^{EB} \equiv \frac{1}{2l+1} \sum_m E_{lm} B_{lm}^*. \quad (5)$$

In the single lens limit, the shear field arising from a scalar gravitational field should be a gradient or curl-free field ($B_{lm} = 0$). The multiple lensing effect generates *B*-mode power spectrum, but their power is $\sim 10^4$ times smaller than the *E*-mode power. Thus the *E*-mode power spectrum effectively contains all information on the cosmic shear, i.e. *E*-mode power spectrum is equivalent to that of the projected mass density along the line-of-sight between source galaxies and an observer. Hence the *B*-mode can be used as a monitor of residual systematic effects. The standard methods to separate *E/B* mode correlation functions involve integrals of the measured correlation functions down to arbitrary small scale or up to very large scale. As the scale range accessible from a finite sky data is limited, residual uncertainties are generated (Schneider et al. 1998; Crittenden et al. 2002, also see Schneider, Eifler & Krause 2010 for a new method using the limited-range integration of correlation function to separate the *E*-mode).

Observational effects, such as a finite sky coverage and bright star masks, limit the survey area to a region $K(\hat{\mathbf{n}})$. The observed shear field is modified as

$$\tilde{\gamma}_1(\hat{\mathbf{n}}) \pm i\tilde{\gamma}_2(\hat{\mathbf{n}}) = K(\hat{\mathbf{n}})(\gamma_1(\hat{\mathbf{n}}) \pm i\gamma_2(\hat{\mathbf{n}})). \quad (6)$$

Without weighting, $K(\hat{\mathbf{n}}) = 0$ if the position vector $\hat{\mathbf{n}}$ lies in masked regions or regions outside the survey, otherwise $K(\hat{\mathbf{n}}) = 1$ within the survey. This finite sky coverage couples modes and generate artificial *B* modes. We can describe the observed shear fields in terms of “pseudo *E* and *B* modes”, denoted as \tilde{E}_{lm} and \tilde{B}_{lm}

$$\tilde{E}_{lm} \pm i\tilde{B}_{lm} = \oint d\Omega_{\hat{\mathbf{n}}} [K(\hat{\mathbf{n}})(\gamma_1(\hat{\mathbf{n}}) \pm i\gamma_2(\hat{\mathbf{n}}))]_{\pm 2} Y_{lm}^*(\hat{\mathbf{n}}). \quad (7)$$

These pseudo \bar{E} and \bar{B} modes are related to the true E and B modes as

$$\tilde{E}_{lm} \pm i\tilde{B}_{lm} = \sum_{l'm'} (E_{l'm'} \pm iB_{l'm'})_{\pm 2} W_{l'mm'}, \quad (8)$$

through a convolution kernel,

$$\begin{aligned} \pm 2 W_{l'mm'} &\equiv \oint d\Omega_{\hat{n}} \pm 2 Y_{l'm'}(\hat{n}) K(\hat{n})_{\pm 2} Y_{lm}^*(\hat{n}) \\ &= \sum_{l''m''} K_{l''m''} (-1)^m \sqrt{\frac{(2l+1)(2l'+1)(2l''+1)}{4\pi}} \\ &\quad \times \begin{pmatrix} l & l' & l'' \\ \pm 2 & \mp 2 & 0 \end{pmatrix} \begin{pmatrix} l & l' & l'' \\ m & m' & m'' \end{pmatrix}, \end{aligned} \quad (9)$$

where $\begin{pmatrix} l_1 & l_2 & l_3 \\ m_1 & m_2 & m_3 \end{pmatrix}$ are known as the Wigner $3j$ symbols (see the references in Dahlen & Tromp 1998) and K_{lm} is the harmonic transform of the mask function $K(\hat{n})$:

$$K_{lm} = \oint d\Omega_{\hat{n}} K(\hat{n}) Y_{lm}^*(\hat{n}). \quad (10)$$

The pseudo power spectra \tilde{C}_l^{EE} , \tilde{C}_l^{BB} and \tilde{C}_l^{EB} are defined similarly to the equations (3)-(5) using pseudo E and B modes (eq.[8]). After straightforward algebraic calculation, one can find that the pseudo and true spectra are related to each other via

$$\tilde{\mathbf{C}}_l = \sum_{l'} \mathbf{M}_{ll'} F_{l'}^2 \mathbf{C}_{l'} + \tilde{\mathbf{N}}_l, \quad (11)$$

where we have introduced the vector notations $\tilde{\mathbf{C}}_l \equiv (\tilde{C}_l^{EE}, \tilde{C}_l^{BB}, \tilde{C}_l^{EB})$ and so on for notational simplicity, and F_l is the pixel window function. In the above equation we include the shot noise contribution arising from the intrinsic ellipticities of source galaxies. The intrinsic noise is simply modeled as the convolved noise power spectrum $\tilde{\mathbf{N}}_l$ with the pixel window and the mask. Non-zero components of the mode-mode coupling matrix $\mathbf{M}_{ll'}$ are given as

$$\begin{aligned} M_{ll'}^{EE,EE} &= M_{ll'}^{BB,BB} \\ &= \frac{2l'+1}{8\pi} \sum_{l''} (2l''+1) \mathcal{K}_{l''} [1 + (-1)^{l+l'+l''}] \\ &\quad \times \begin{pmatrix} l & l' & l'' \\ 2 & -2 & 0 \end{pmatrix}^2, \end{aligned} \quad (12)$$

$$\begin{aligned} M_{ll'}^{EE,BB} &= M_{ll'}^{BB,EE} \\ &= \frac{2l'+1}{8\pi} \sum_{l''} (2l''+1) \mathcal{K}_{l''} [1 - (-1)^{l+l'+l''}] \\ &\quad \times \begin{pmatrix} l & l' & l'' \\ 2 & -2 & 0 \end{pmatrix}^2, \end{aligned} \quad (13)$$

$$M_{ll'}^{EB,EB} = \frac{2l'+1}{4\pi} \sum_{l''} (2l''+1) \mathcal{K}_{l''} \begin{pmatrix} l & l' & l'' \\ 2 & -2 & 0 \end{pmatrix}^2, \quad (14)$$

with \mathcal{K}_l being defined as

$$\mathcal{K}_l \equiv \frac{1}{2l+1} \sum_m K_{lm} K_{lm}^*. \quad (15)$$

Note that $M_{ll'}^{EE,EB} = 0 = M_{ll'}^{BB,EB}$. Equation (11) tells that an imperfect survey geometry causes mode-mixing or

equivalently a leakage of E -mode power into the B -mode even if $C_l^{BB} = 0$.

The underlying power spectra can be reconstructed by solving the equation (11) inversely. The resolution in multipole space is limited by the survey area, i.e. the finer binning less than $l_f \equiv \sqrt{\pi/f_{\text{sky}}}$ does not improve the statistical significance of the power spectrum reconstruction. Since the lensing power spectrum does not have fine scale structures in multipole space, such a coarse binning is sufficient to capture the shape of shear power spectrum. Also the coarse binning significantly reduces the computational cost of measuring the power spectrum in a wide range of multipoles. We therefore measure the binned power spectra defined as

$$\mathbf{C}_b \equiv \sum_l^{l \in b} P_{bl} \mathbf{C}_l, \quad (16)$$

where the index “ b ” denotes the b -th multipole bin, and $\sum_l^{l \in b}$ represents the summation over l between $l_{\min}^{(b)}$ and $l_{\min}^{(b+1)} - 1$. Here we use a binned operator P_{bl} so that the binned power becomes the average of dimensionless power over l between $l_{\min}^{(b)}$ to $l_{\min}^{(b+1)} - 1$

$$P_{bl} \equiv \frac{l(l+1)}{2\pi} \frac{1}{l_{\min}^{(b+1)} - l_{\min}^{(b)}}. \quad (17)$$

The deconvolved binned spectrum is obtained as

$$\mathbf{C}_b = (\mathbf{M}^{-1})_{bb'} \sum_l^{l \in b'} P_{b'l} (\tilde{\mathbf{C}}_l - \tilde{\mathbf{N}}_l)_{\text{MC}}. \quad (18)$$

The mode mixing matrix for the binned spectra is

$$\mathbf{M}_{bb'} = \sum_l^{l \in b} P_{bl} \sum_{l'}^{l' \in b'} \mathbf{M}_{ll'} F_{l'}^2 Q_{l'b'}, \quad (19)$$

where Q_{lb} is the reciprocal of P_{bl}

$$Q_{lb} \equiv \frac{2\pi}{l(l+1)}. \quad (20)$$

The equation (18) is the key equation for reconstructing the shear power spectra from masked shear maps in the full-sky approach in Section 4.

2.2 Flat-Sky Approximation

In this subsection, we present a formalism of a pseudo-spectrum method in the flat-sky approximation. The flat-sky approximation is enough applicable to current lensing survey, such as the CFHT survey covering a sky of about 200 square degrees in its 4 survey regions (e.g. Fu et al. 2008).

In the flat-sky approximation, E and B modes are defined as

$$E_{\mathbf{k}}^{\text{flat}} \pm iB_{\mathbf{k}}^{\text{flat}} = \int d\Omega_{\mathbf{n}} [\gamma_1(\mathbf{n}) \pm i\gamma_2(\mathbf{n})] e^{-i(\mathbf{k} \cdot \mathbf{n} \pm 2\varphi_{\mathbf{k}})}, \quad (21)$$

and inversely related as

$$\gamma_1(\mathbf{n}) \pm i\gamma_2(\mathbf{n}) = \int \frac{d^2\mathbf{k}}{(2\pi)^2} [E_{\mathbf{k}}^{\text{flat}} \pm iB_{\mathbf{k}}^{\text{flat}}] e^{i(\mathbf{k} \cdot \mathbf{n} \pm 2\varphi_{\mathbf{k}})}, \quad (22)$$

where the vector \mathbf{n} is a flat-space two-dimensional vector that approximates the three-dimensional vector $\hat{\mathbf{n}}$ in Eq. (1) around some reference point; e.g., if the coordinate origin in

flat space is taken as the north pole, the position vector of an arbitrary point in the vicinity of the north pole is specified by two-dimensional vector $\mathbf{n} = \theta(\cos \varphi, \sin \varphi) = (\theta_x, \theta_y)$. The vector \mathbf{k} is the corresponding wavenumber in the flat-space coordinate, and $\varphi_{\mathbf{k}}$ is defined as $\mathbf{k} = k(\cos \varphi_{\mathbf{k}}, \sin \varphi_{\mathbf{k}})$.

Like in the full-sky formalism, we again define pseudo E and B modes in a flat-sky limit as

$$\tilde{E}_{\mathbf{k}}^{\text{flat}} \pm i\tilde{B}_{\mathbf{k}}^{\text{flat}} = \int d\Omega_{\mathbf{n}} [W(\mathbf{n})(\gamma_1(\mathbf{n}) \pm i\gamma_2(\mathbf{n}))] e^{i(\mathbf{k}\cdot\mathbf{n} \pm 2\varphi_{\mathbf{k}})}, \quad (23)$$

where W represents an arbitrary mask field. We take into account the mask effect in two steps: a square boundary covering observed survey regions and the mask inside the square. Even for a complex survey geometry, such a square shape geometry can be obtained by using the zero-padding method such that the square-shape region encloses the whole region of data.

The pseudo E/B-mode coefficient $\hat{E}_{\mathbf{k}}^{\text{flat}} \pm i\hat{B}_{\mathbf{k}}^{\text{flat}}$ for a square field of a side length L relate to the underlying true coefficients $E_{\mathbf{k}}^{\text{flat}} \pm iB_{\mathbf{k}}^{\text{flat}}$ as (Bunn 2002)

$$\hat{E}_{\mathbf{k}}^{\text{flat}} \pm i\hat{B}_{\mathbf{k}}^{\text{flat}} = \int \frac{d^2\mathbf{k}'}{(2\pi)^2} (E_{\mathbf{k}'}^{\text{flat}} \pm iB_{\mathbf{k}'}^{\text{flat}}) S_{\mathbf{k}-\mathbf{k}'} e^{\pm 2i\varphi_{\mathbf{k}'}}, \quad (24)$$

where $S_{\mathbf{k}}$ is the Fourier transform of the survey window function defined as

$$S_{\mathbf{k}} = \frac{\sin(k_x L/2)}{k_x/2} \frac{\sin(k_y L/2)}{k_y/2}, \quad (25)$$

and $k_x(k_y)$ are $x(y)$ -components of \mathbf{k} . The window function $S_{\mathbf{k}}$ approaches L^2 as \mathbf{k} goes to $\mathbf{0}$.

The shear power spectra in flat-sky approximation is defined as

$$\begin{aligned} \langle E_{\mathbf{k}}^{\text{flat}} E_{\mathbf{k}'}^{\text{flat}*} \rangle &\equiv (2\pi)^2 \delta_D^2(\mathbf{k} + \mathbf{k}') C_k^{EE} \\ \langle B_{\mathbf{k}}^{\text{flat}} B_{\mathbf{k}'}^{\text{flat}*} \rangle &\equiv (2\pi)^2 \delta_D^2(\mathbf{k} + \mathbf{k}') C_k^{BB} \\ \langle E_{\mathbf{k}}^{\text{flat}} B_{\mathbf{k}'}^{\text{flat}*} \rangle &\equiv (2\pi)^2 \delta_D^2(\mathbf{k} + \mathbf{k}') C_k^{EB} \end{aligned} \quad (26)$$

Here $\delta_D^2(\mathbf{k})$ is the two-dimensional Dirac delta function. From Eq. (24) the pseudo power spectra for the square area relate to the true one as

$$\begin{aligned} \hat{C}_{\mathbf{k}}^{EE} &\equiv L^{-2} \langle |\hat{E}_{\mathbf{k}}^{\text{flat}}|^2 \rangle \\ &= \int \frac{d^2\mathbf{k}'}{(2\pi)^2} S_{\mathbf{k}-\mathbf{k}'} [\cos^2(2\varphi_{\mathbf{k}'}) C_{\mathbf{k}'}^{EE} + \sin^2(2\varphi_{\mathbf{k}'}) C_{\mathbf{k}'}^{BB}], \\ \hat{C}_{\mathbf{k}}^{BB} &\equiv L^{-2} \langle |\hat{B}_{\mathbf{k}}^{\text{flat}}|^2 \rangle \\ &= \int \frac{d^2\mathbf{k}'}{(2\pi)^2} S_{\mathbf{k}-\mathbf{k}'} [\sin^2(2\varphi_{\mathbf{k}'}) C_{\mathbf{k}'}^{EE} + \cos^2(2\varphi_{\mathbf{k}'}) C_{\mathbf{k}'}^{BB}], \\ \hat{C}_{\mathbf{k}}^{EB} &\equiv L^{-2} \langle \hat{E}_{\mathbf{k}}^{\text{flat}} \hat{B}_{-\mathbf{k}}^{\text{flat}} \rangle \\ &= \int \frac{d^2\mathbf{k}'}{(2\pi)^2} S_{\mathbf{k}-\mathbf{k}'} [\cos^2(2\varphi_{\mathbf{k}'}) - \sin^2(2\varphi_{\mathbf{k}'})] C_{\mathbf{k}'}^{EB}, \end{aligned} \quad (27)$$

where $\varphi_{\mathbf{k}'\mathbf{k}} \equiv \varphi_{\mathbf{k}'} - \varphi_{\mathbf{k}}$ and $S_{\mathbf{k}}$ is the power spectrum of $S_{\mathbf{k}}$ defined as

$$\langle S_{\mathbf{k}} S_{\mathbf{k}'}^* \rangle \equiv (2\pi)^2 \delta_D^2(\mathbf{k} + \mathbf{k}') S_{\mathbf{k}}. \quad (28)$$

The pseudo spectrum in the equation (27) depend on wavevector \mathbf{k} rather than its length. We later introduce the azimuthal angle average over $\varphi_{\mathbf{k}}$ in reconstructing the true spectra $C_{\mathbf{k}}$ that depend only on the length of wavevector \mathbf{k} .

Although the relations between the pseudo and underlying spectra involve an infinite-range integral, we find that

the equation (27) can be approximated by the following algebraical relations via the mode-mixing matrix:

$$\hat{\mathbf{C}}_{\mathbf{k}}^{\text{flat}} = \sum_{\mathbf{k}'} \mathbf{M}_{\mathbf{k}\mathbf{k}'}^{\mathcal{S}} \mathbf{C}_{\mathbf{k}'}^{\text{flat}}. \quad (29)$$

Non-zero components of the mode-mixing matrix are given using the power spectrum of the power spectrum of survey window $S_{\mathbf{k}}$ (eq.[28]) as

$$\begin{aligned} M_{\mathbf{k}\mathbf{k}'}^{SEE,EE} &= M_{\mathbf{k}\mathbf{k}'}^{SBB,BB} \simeq \overline{S}_{\mathbf{k}\mathbf{k}'}^{(\cos 2)}, \\ M_{\mathbf{k}\mathbf{k}'}^{SEE,BB} &= M_{\mathbf{k}\mathbf{k}'}^{SBB,EE} \simeq \overline{S}_{\mathbf{k}\mathbf{k}'}^{(\sin 2)}, \\ M_{\mathbf{k}\mathbf{k}'}^{SEB,EB} &\simeq \overline{S}_{\mathbf{k}\mathbf{k}'}^{(\cos 2)} - \overline{S}_{\mathbf{k}\mathbf{k}'}^{(\sin 2)}, \end{aligned} \quad (30)$$

where

$$\begin{aligned} \overline{S}_{\mathbf{k}\mathbf{k}'}^{(\cos 2)} &= \int_{k'_x - \pi/L}^{k'_x + \pi/L} \frac{dk'_x}{2\pi} \int_{k'_y - \pi/L}^{k'_y + \pi/L} \frac{dk'_y}{2\pi} S_{\mathbf{k}-\mathbf{k}'} \cos^2(2\varphi_{\mathbf{k}'\mathbf{k}}), \\ \overline{S}_{\mathbf{k}\mathbf{k}'}^{(\sin 2)} &= \int_{k'_x - \pi/L}^{k'_x + \pi/L} \frac{dk'_x}{2\pi} \int_{k'_y - \pi/L}^{k'_y + \pi/L} \frac{dk'_y}{2\pi} S_{\mathbf{k}-\mathbf{k}'} \sin^2(2\varphi_{\mathbf{k}'\mathbf{k}}). \end{aligned} \quad (31)$$

Note $M^{SEE,EB} = 0 = M^{SBB,EB}$ as in the full-sky approach. Since the discrete Fourier decomposition is limited by the resolution of survey size L , we approximate the mode-mixing matrix as an average of the survey window function multiplied with either of $\cos^2(2\varphi_{\mathbf{k}\mathbf{k}'})$ or $\sin^2(2\varphi_{\mathbf{k}\mathbf{k}'})$ over a single pixel of area $(2\pi/L)^2$ around the vector \mathbf{k}' in Fourier space. The mode-mixing due to the survey window is important particularly for large-scale modes ($k \sim 2\pi/L$).

We further need to include the masking effect inside the square boundary. As in the full-sky approach, the Fourier coefficients of the shear field with the inside mask $K(\mathbf{n})$ is related to those without the mask as

$$\tilde{E}_{\mathbf{k}}^{\text{flat}} \pm i\tilde{B}_{\mathbf{k}}^{\text{flat}} = \sum_{\mathbf{k}'} (\hat{E}_{\mathbf{k}'}^{\text{flat}} \pm i\hat{B}_{\mathbf{k}'}^{\text{flat}}) \pm_2 W_{\mathbf{k}'\mathbf{k}}, \quad (32)$$

where the convolution kernel $\pm_2 W_{\mathbf{k}'\mathbf{k}}$ is given in terms of the Fourier transform of the mask function, $K_{\mathbf{k}}$, as

$$\pm_2 W_{\mathbf{k}'\mathbf{k}} \equiv L^{-2} K_{\mathbf{k}-\mathbf{k}'} e^{\pm 2i\varphi_{\mathbf{k}'\mathbf{k}}}. \quad (33)$$

In the equation (32) we use the discrete summation, rather than the infinite-range Fourier transform. The summation runs over the Fourier-space grids where the resolution of each grid is specified by the square size L as $(2\pi/L)^2$. The number of grids, N_{grid}^2 , needs to be specified by an observer to achieve the desired coverage of multipole range.

The pseudo spectra $\hat{\mathbf{C}}_{\mathbf{k}}^{\text{flat}}$ for the masked field inside the square boundary is

$$\tilde{\mathbf{C}}_{\mathbf{k}}^{\text{flat}} = \sum_{\mathbf{k}'} \mathbf{M}_{\mathbf{k}\mathbf{k}'}^{\mathcal{K}} \hat{\mathbf{C}}_{\mathbf{k}'}^{\text{flat}}, \quad (34)$$

The mode-coupling matrix for the masking effect is given by

$$M_{\mathbf{k}\mathbf{k}'}^{\mathcal{K}EE,EE} = M_{\mathbf{k}\mathbf{k}'}^{\mathcal{K}BB,BB} = L^{-2} \mathcal{K}_{\mathbf{k}-\mathbf{k}'} \cos^2(2\varphi_{\mathbf{k}'\mathbf{k}}), \quad (35)$$

$$M_{\mathbf{k}\mathbf{k}'}^{\mathcal{K}EE,BB} = M_{\mathbf{k}\mathbf{k}'}^{\mathcal{K}BB,EE} = L^{-2} \mathcal{K}_{\mathbf{k}-\mathbf{k}'} \sin^2(2\varphi_{\mathbf{k}'\mathbf{k}}), \quad (36)$$

$$M_{\mathbf{k}\mathbf{k}'}^{\mathcal{K}EB,EB} = L^{-2} \mathcal{K}_{\mathbf{k}-\mathbf{k}'} [\cos^2(2\varphi_{\mathbf{k}'\mathbf{k}}) - \sin^2(2\varphi_{\mathbf{k}'\mathbf{k}})] \quad (37)$$

where $\mathcal{K}_{\mathbf{k}}$ is the power spectrum of the mask field inside the square boundary

$$\langle K_{\mathbf{k}} K_{\mathbf{k}'}^* \rangle \equiv L^2 \delta_{\mathbf{k}-\mathbf{k}'}^{\mathcal{K}} \mathcal{K}_{\mathbf{k}}. \quad (38)$$

Combining the equations (29) and (34), the pseudo spectra $\tilde{C}_k^{\text{flat}}$ is related to the true underlying spectra as

$$\tilde{C}_k^{\text{flat}} = \sum_{k''} M_{kk''}^{\mathcal{C}} \sum_{k'} M_{k''k'}^{\mathcal{S}} C_{k'}^{\text{flat}}. \quad (39)$$

We compute the binned power spectra:

$$\tilde{C}_b^{\text{flat}} \equiv \sum_{\mathbf{k}}^{k \in b} P_{bk} \tilde{C}_{\mathbf{k}}^{\text{flat}}, \quad (40)$$

where the summation corresponds to an azimuthal angle average of \mathbf{k} , and runs over all the Fourier modes satisfying the condition $|\mathbf{k}| \in [k_b, k_{b+1}]$. The operator P_{bk} is defined to average dimensionless power within the bin of scales

$$P_{bk} = \frac{1}{\nu_b} \frac{k^2}{2\pi}, \quad (41)$$

and its reciprocal is

$$Q_{kb} = \frac{2\pi}{k^2}. \quad (42)$$

The quantity ν_b is the number of Fourier modes available for the b -th multipole bin, and is approximately given for a mode of $k \gg 1/L$ as

$$\nu_b \equiv \sum_{\mathbf{k}}^{k \in b} \simeq 2\pi k (k_{\text{low}}^{(b+1)} - k_{\text{low}}^{(b)}). \quad (43)$$

Therefore, as in the full-sky approach, the underlying power spectra can be estimated by deconvolving the pseudo power spectra in the flat-sky approximation:

$$C_b^{\text{flat}} \simeq (\mathbf{M}^{-1})_{bb'} \sum_{\mathbf{k}}^{k \in b'} P_{b'k} (\tilde{C}_{\mathbf{k}}^{\text{flat}} - \langle \tilde{\mathbf{N}}_{\mathbf{k}} \rangle_{\text{MC}}), \quad (44)$$

where the mode mixing matrix is given as

$$\mathbf{M}_{bb'} = \sum_{b''} M_{bb''}^{\mathcal{C}} M_{b''b'}^{\mathcal{S}}. \quad (45)$$

with

$$\begin{aligned} M_{bb'}^{\mathcal{S}} &= \sum_{\mathbf{k}}^{k \in b} P_{bk} \sum_{\mathbf{k}'}^{k' \in b'} M_{\mathbf{k}\mathbf{k}'}^{\mathcal{S}} Q_{k'b'}, \\ M_{bb'}^{\mathcal{C}} &= \sum_{\mathbf{k}}^{k \in b} P_{bk} \sum_{\mathbf{k}'}^{k' \in b'} M_{\mathbf{k}\mathbf{k}'}^{\mathcal{C}} Q_{k'b'}. \end{aligned} \quad (46)$$

We use the equation (44) to reconstruct the power spectra from the pseudo spectra in the flat-sky approximation.

3 SIMULATIONS OF SHEAR MAPS

We use simulated maps of shear fields to test the pseudo-spectrum technique for reconstructing the shear power spectrum. We address how the method works for the case of lensing maps, where the lensing power spectrum has distinct shapes from the CMB power spectrum: the lensing spectrum has greater amplitudes at smaller scales. We also study the validity of the flat-sky approximation for recovering the input power spectrum down to very small angular scales in the presence of the finite-sky survey and masking effects.

3.1 Simulating the Lensed Sky

We construct two types of simulated shear fields: flat-sky non-Gaussian fields from ray-tracing simulations to test the flat-sky method and full-sky Gaussian fields to test the full-sky deconvolution method.

3.1.1 Full Simulations in Flat-Sky Limit

We use the shear maps constructed from ray-tracing simulations developed by Sato et al. (2009) and test the flat-sky deconvolution method. The ray-tracing simulations are performed by placing N-body simulation boxes with two different sizes ($240h^{-1}\text{Mpc}$ and $480h^{-1}\text{Mpc}$ at a side length) to cover a light cone of angular size $5^\circ \times 5^\circ$ from $z=0$ to 3.5. The N-body simulations are based on the parallel Tree-Particle Mesh code Gadget-2 (Springel 2005). The ray-tracing simulation follows the standard multiple lens plane algorithm (Jain, Seljak & White 2000; Hamana & Mellier 2001): separating the comoving distance between an observer and a source by fixed intervals of $120h^{-1}\text{Mpc}$, computing the projected density contrast at each lens plane along the line-of-sight, we obtain the two-dimensional gravitational potential field related to the density contrast via Poisson equation. In this paper we use the simulations with a single source redshift $z = 1$. The initial ray directions are set on 2048×2048 Cartesian grids (resolution $300/2048 \simeq 0.15$ [arcmin]) and the ray positions at each lens plane are traced backward to the source plane via the lens equation. We obtain the shear field from the Jacobian matrix describing deformation of an infinitesimal light ray bundle. It should be noted that the obtained shear field does not obey the periodic boundary condition due to the projection to a single observer point through the different simulation boxes. The fundamental mode of the shear field is given by $l_f = 2\pi/L = 72$ with $L = (5/180)\pi$. We use 1000 realizations of the shear maps in order to sufficiently reduce statistical scatters in the measured power spectra.

We adopt the concordance ΛCDM model: the present-day density parameters of matter, cosmological constant, and baryon are $\Omega_m = 0.238$, $\Omega_\Lambda = 0.762$, and $\Omega_b = 0.042$, respectively; the Hubble parameter $H_0 = 73.2 \text{ km s}^{-1} \text{ Mpc}^{-1}$; the spectral index $n_s = 0.958$; the rms density fluctuations in a sphere of $8h^{-1}\text{Mpc}$ radius $\sigma_8 = 0.76$ used for the power spectrum normalization (Spergel et al. 2007).

3.1.2 Gaussian Simulations in Full-Sky Limit

To test the full-sky formalism (Sec. 2.1), we construct Gaussian shear fields using the HEALPix software (Górski et al. 2005). We assume the survey geometry to be a rectangular shape covering 2000 square degree (see the top panel of Fig. 1). The resolution parameter of HEALPix pixelization N_{side} is set to be 1024 corresponding to ~ 4 arcmin for the pixel scale and the maximum multipole $l_{\text{max}} = 2000$.

The spectrum of the shear fields is of E -mode only assuming the concordance cosmological model same as the N-body simulations (Sec. 3.1.1). In the weak lensing limit, the E -mode shear power spectrum C_l^{EE} is equivalent to the power spectrum of lensing convergence field, the weighted mass density field projected between source galaxies and an

observer along the line-of-sight. Assuming the Limber’s approximation (Limber 1954), the E -mode power spectrum is simply expressed as a weighted projection of the the matter power spectrum $P_\delta(k)$:

$$C_l^{EE} = \int_0^\infty dr r^{-2} W_{\text{GL}}^2(r) P_\delta\left(k = \frac{l}{r}; z\right), \quad (47)$$

where r is the comoving angular diameter distance, and we throughout this paper assume a flat universe. Note that the comoving distance is given as a function of redshift, i.e. the distance-redshift relation $r = r(z)$. The lensing efficiency function, $W_{\text{GL}}(r)$, is given by

$$W_{\text{GL}}(r) \equiv \frac{3}{2} \left(\frac{H_0}{c}\right)^2 \Omega_m a^{-1} r \int_r^\infty dr' G(r') \frac{r' - r}{r'}, \quad (48)$$

where $G(r)dr = p(z)dz$ is the normalized source distribution and

$$p(z) \propto \delta_D(z - z_s) \quad (49)$$

with $z_s = 1$.

3.2 Simulating Realistic Masks

We consider three types of masks typical for ground-based imaging data analyses: point sources, saturation spikes, and bad pixels. First masked regions have circular shapes to model “bright stars” that are randomly distributed in the shear map. The radii of the bright star masks are randomly chosen ranging from 0.2 to 2 arcminutes. When the radius of the circle is greater than 1 arcmin, we add a rectangular-shape mask to model “saturation spikes” around a bright star. The mask has the size of $0.2r \times 5r$ (r is the radius of masked circle) with the same center as the circle. The different masked regions are allowed to be overlapped. We also mask all the pixels in a y -direction row randomly selected with 5% probability. About 25% fraction of the area is totally masked in each simulation realization, which is typical for a ground-based imaging survey such as the Subaru Telescope (Hamana et al. 2003). The configuration of masked regions is demonstrated in the bottom panel of Fig. 1.

Since the pixel size of the ray-tracing simulations (0.15 arcmin) is smaller than the bright star mask, the mask function $K(\mathbf{n})$ is set as $K = 0$ when the center of the pixel is masked, otherwise 1. The middle panel of Fig. 1 shows a typical configuration of the simulated map with mask, while the spatial resolution is degraded in the plot. On the other hand, the Gaussian simulations have a large pixel size (4 arcmin) compared to the bright star mask, the mask function $K(\mathbf{n})$ has a fractional value. Besides this difference the masking configuration is kept same in all the realizations for both the full-sky and flat-sky simulations.

3.3 Intrinsic Ellipticities

The intrinsic ellipticities of source galaxy shapes generate a white noise contamination to the power spectrum measurement assuming random orientations between different galaxies:

$$N_l = \frac{\sigma_\epsilon^2}{\bar{n}_g}, \quad (50)$$

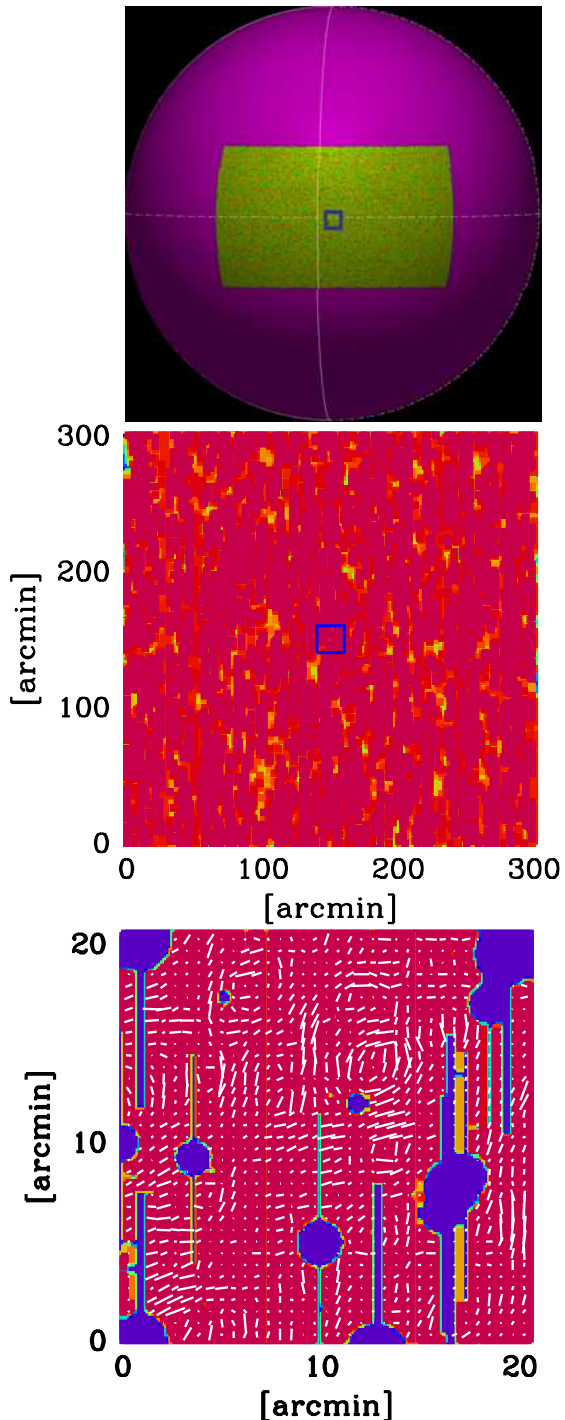


Figure 1. *Top panel:* A representative realization of the full-sky simulations assuming that the shear field is Gaussian. The simulated survey geometry is a rectangular shape with 2000 sq. deg. area. *Middle panel:* Similarly, but for the flat-sky approximation, which is done by ray-tracing simulations based on N-body simulations for the concordance Λ CDM model. The simulated map has a square shape with 25 sq. deg. area (the corresponding area is displayed by the square line in the upper panel). *Bottom panel:* A typical configuration of masked regions in a patch of 20×20 arcmin² (the corresponding area is displayed by the square line in the middle panels). The masked regions occupy about 25% of the total simulated area.

where σ_ϵ is the rms ellipticities per component and \bar{n}_g is the mean number density of source galaxies. In the following we assume $\sigma_\epsilon = 0.22$ and $\bar{n}_g = 30 \text{ arcmin}^{-2}$.

After masking the simulated shear fields, we add a Gaussian random noise with the variance of $\sigma_\epsilon^2/(\bar{n}_g\Omega_{\text{pix}})$ to each pixel, where Ω_{pix} is the pixel size. For Gaussian simulations, we add an effective noise with the variance of $\sigma_\epsilon^2/(f_{\text{pix}}\bar{n}_g\Omega_{\text{pix}})$ to pixels inside the survey area, where f_{pix} denotes the unmasked fraction roughly equal to 0.75.

4 RESULTS

4.1 Power Spectrum Reconstruction

Fig. 2 shows the results of the shear spectrum reconstruction in the flat-sky approximation using 1000 realizations of the ray-tracing simulation. The left panel shows the noiseless results, while the right panel shows the results with intrinsic ellipticity. The shot noise spectra are subtracted from the measured spectra using the theoretical prediction (Eq. [50]) in this plot. In reality the shot noise spectra can be estimated by erasing the coherent cosmic shear signals in each galaxy shape, e.g. by remeasuring the shear spectra after randomly rotating orientations of each galaxy.

Middle panels in Fig. 2 plot the E -mode power spectrum. The solid curve denotes the input power spectrum, while the dashed curve is the convolved spectrum, i.e. the measured power spectrum from the simulated shear maps without correcting for the survey geometry effect. The convolved spectrum systematically underestimates the underlying amplitudes over all the scales. On angular scales larger than a typical scale of masked areas (small l), the amplitude offset is roughly determined by the square of the masked area fraction i.e. $0.75 \times 0.75 \simeq 0.56$. On the other hand, the offset on larger l is given by the area fraction, 0.75. The modes, which angular scale is larger than the mask size, is fractionally affected by the mask and thus the amplitude decreases proportional to the masked fraction. Their power is thereby proportional to the square of the unmasked fraction. On the other hand, when the scale of modes is much smaller than the mask size, their amplitude is 0 in masked region or 1 in unmasked region. As a result, their square value also has a value of 0 or 1 and thus the power is proportional just to the unmasked fraction (not the square).

The triangle symbols show the mean pseudo power spectra over 1000 realizations of the shear maps and the circle symbols are the deconvolved one. The error-bars represent the expected 1σ statistical errors of the band powers for a 2000 square degree survey. Since the ray-tracing simulation has the area of 25 square degree, we estimate the errors by multiplying the measured scatters among 1000 realizations with a factor $\sqrt{2000/25}$. We set the binning width wider than the fundamental mode $l_f = 2\pi/L = 72$: the first 10 bins have linearly equal spacing as $l_{\text{min}}^{(b)} = 0.6l_f + 1.2l_fb$, while the remaining 25 bins have logarithmically equal spacing up to $l_{\text{max}} = 10000$. Our reconstruction method successfully recovers the input E -mode spectrum for both cases without intrinsic noise (left panels) and with noise (right panels). The top panel explicitly shows the ratio of the reconstructed E -mode power spectra to the input spectrum. The accuracy

of the reconstruction achieves a sub-percent level over the most ranges of multipoles.

The lower panels show the B -mode power spectrum relative to the E -mode spectrum. The mask and finite-sky effect generates B -mode due to the mode mixing. In fact, there is a significant leakage of the E -mode into the B -mode ($\sim 10\%$ of E -mode power) as shown in triangle symbols. We find that the leakage disappears to be less than one percent after deconvolution (see the filled circle symbols).

Fig. 3 shows the results of the full-sky approach (Sec. 2.1) using 1000 Monte Carlo simulations of Gaussian shear fields. The error-bars represent 1σ statistical dispersion for a survey with 2000 square degree coverage. The binning width is set to be wider than $l_f = \sqrt{\pi/f_{\text{sky}}} \sim 8$: the first 10 bins have linearly equal spacing as $l_{\text{min}}^{(b)} = 2 + 10 \times b$ with, while the remaining 20 bins have logarithmically equal spacing up to $l_{\text{max}} = 2000$. The power at the lowest bin ($12 \leq l < 22$) is affected by the unseen modes larger than the surveyed region and thus the reconstructed power at the lowest bin varies with the chosen minimum l and the binning width. When the minimum l is taken to be slightly larger than l_f , we find that the reconstructed power becomes almost equal to the input power. The accuracy is limited by the statistical errors due to insufficient sampling of such large-angle modes. The power spectrum without correcting for a finite-sky effect (dashed line) is smaller than the input power spectrum (solid line). The amplitude offset is roughly determined by the square of unmasked fraction times the survey area fraction, $0.75 \times 0.75 \times 2000$ square degree divided by 4π steradian, that is about 0.028.

Summarizing the results in Figs. 2 and 3 the pseudo-spectrum method recovers the input power spectrum at a sub-percent accuracy over a wide range of multipoles down to $l \simeq 10^4$. As seen from the top panels, the ratio between the true and reconstructed spectra is close to unity over a range of multipoles we study. The scatters of the ratio from unity imply possible biases in the E -mode power spectrum reconstruction at each multipole bin, and are smaller than the statistical errors of power spectrum measurement expected for a survey of 2000 sq. deg. coverage. The residual B -mode power spectrum is suppressed below a percent level.

4.2 Correlated Spectrum Errors due to the Mode Mixing

Finite-sky effect makes the errors of the shear power spectra correlate between different bins. In this subsection we study this effect using the simulated maps.

Let's start our discussion using Gaussian fields. The statistical errors of the binned power spectrum is given, in the absence of shot noise, as

$$\Delta C_b^{(\text{Gauss})} = C_b \sqrt{\frac{2}{f_{\text{sky}} \nu_b}}, \quad (51)$$

where f_{sky} is the sky fraction of survey area and ν_b is the number of modes available around the b -th bin.

The left panel of Fig. 4 compares the Gaussian expectation (51) with the statistical errors in the E -mode power spectrum of 1000 Gaussian shear fields. When the multipole bin width is taken as $\Delta l = 20, 2.5$ times wider than the fundamental mode $l_f \equiv \sqrt{\pi/f_{\text{sky}}} \simeq 8$, the errors for the

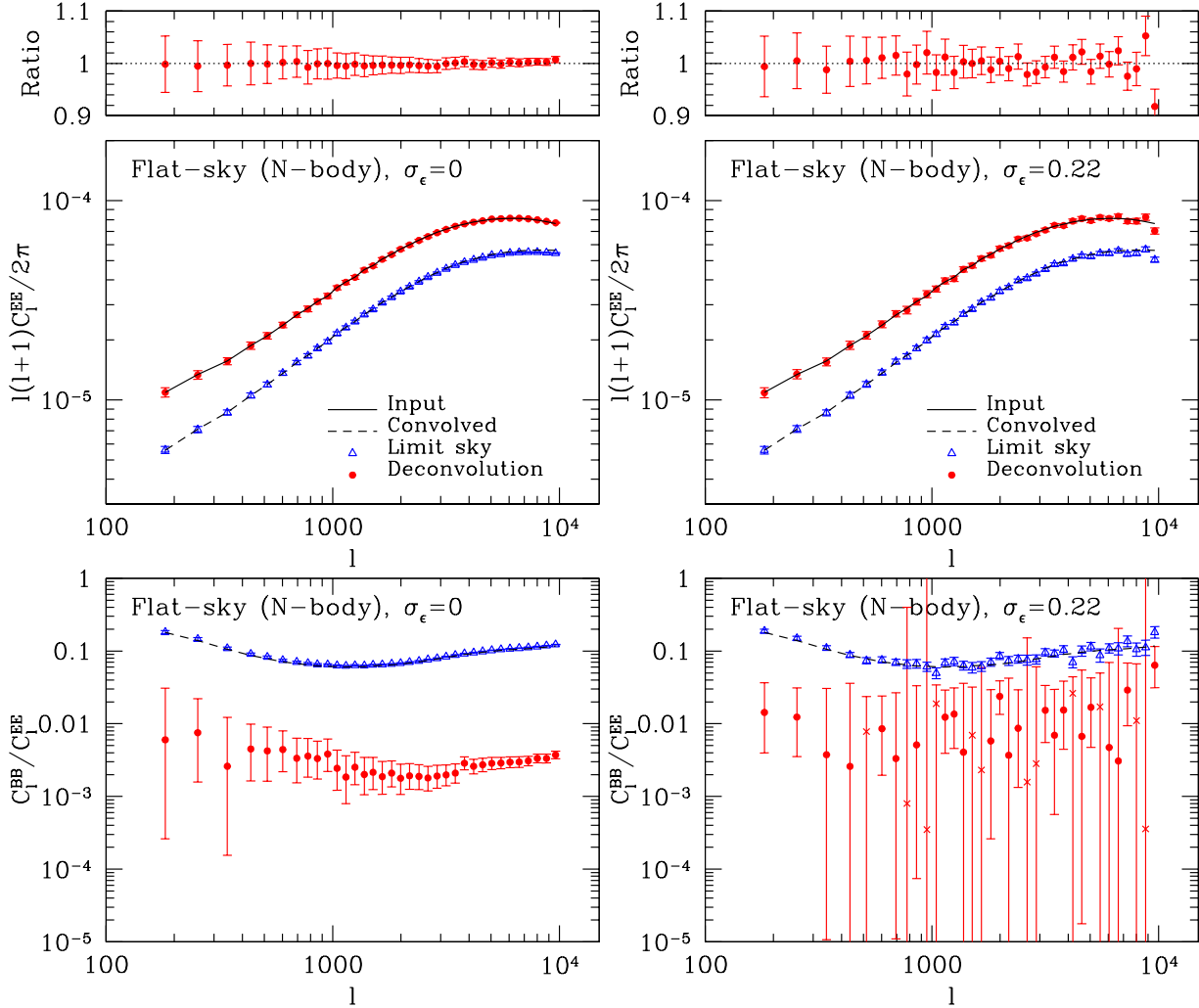


Figure 2. Shear power spectra averaged over 1000 realizations of the ray-tracing simulations. Left panels show the noise-free results, while right panels show the results with the intrinsic shape noise. Note that the theoretical prediction for the shot noise power spectrum (see Eq. [50]) is subtracted from the measured power spectra. *Middle panel:* The solid lines show the input convergence power spectrum. The triangle symbols are the pseudo E -mode power spectrum directly measured from the masked simulations (without correcting for the survey geometry effect), which significantly underestimate the input power spectrum denoted by the solid curve. The dashed lines show the theoretical pseudo spectrum obtained by convolving the input spectrum with the mask. The circle symbols show the reconstructed E -mode power spectra correcting for the survey geometry effect based on the method in Sec. 2.2. As explicitly shown in the top panel, the reconstructed E -mode spectrum agrees with the input spectrum at a sub-percent level over a wide range of multipoles down to $\ell = 10^4$. The deviation is much smaller than the expected statistical errors for a survey of 2000 square degree area coverage denoted by the error-bars. The errors are estimated by scaling the measured scatters of the original simulations, which has 25 sq. degree area, with a factor $\sqrt{2000/25}$. *Bottom panel:* The B -mode power spectra before and after correcting for the survey geometry effects, compared with the corresponding E -mode spectra. Note that the B -mode spectrum can be negative after multiplying the mode-mixing matrix with the measured E/B -mode spectra, and the cross symbols denote such negative B -mode values. The reconstruction method suppresses the residual B -mode below a percent level shown by the circle symbols.

simulation results are greater than the Gaussian expectation. The limit of sky area and mask causes correlated errors between neighboring multipole bins and increases the errors by 10-20% over a range of multipoles. When the bin width is enough wide such as $\Delta l = 100 \gtrsim 12.5l_f$, the power spectrum errors become similar to the Gaussian expectations, and the spectra at different bins become nearly independent.

The right panel of Fig. 4 compares the error of the reconstructed shear power relative to the unmasked convergence power using the ray-tracing simulations, which contain the non-Gaussian error due to nonlinear clustering in

structure formation. At a bin width $\Delta l = 200$, a factor 3 wider than the fundamental mode $l_f = 72$, the power spectrum errors increase by about 5% on small multipoles, while the correlated errors are well suppressed at a wider binning $\Delta l = 1000 \sim 10l_f$. Note that the Gaussian errors depend on the bin width of multipoles, while the non-Gaussian errors do not: a wider bin relatively suppresses the Gaussian error contribution. As studied in Takada & Jain (2009) (also see Sato et al. 2009), the non-Gaussian error contribution is significant at multipoles $\ell \gtrsim 1000$ for the Λ CDM model.

Since most of useful cosmological information in the

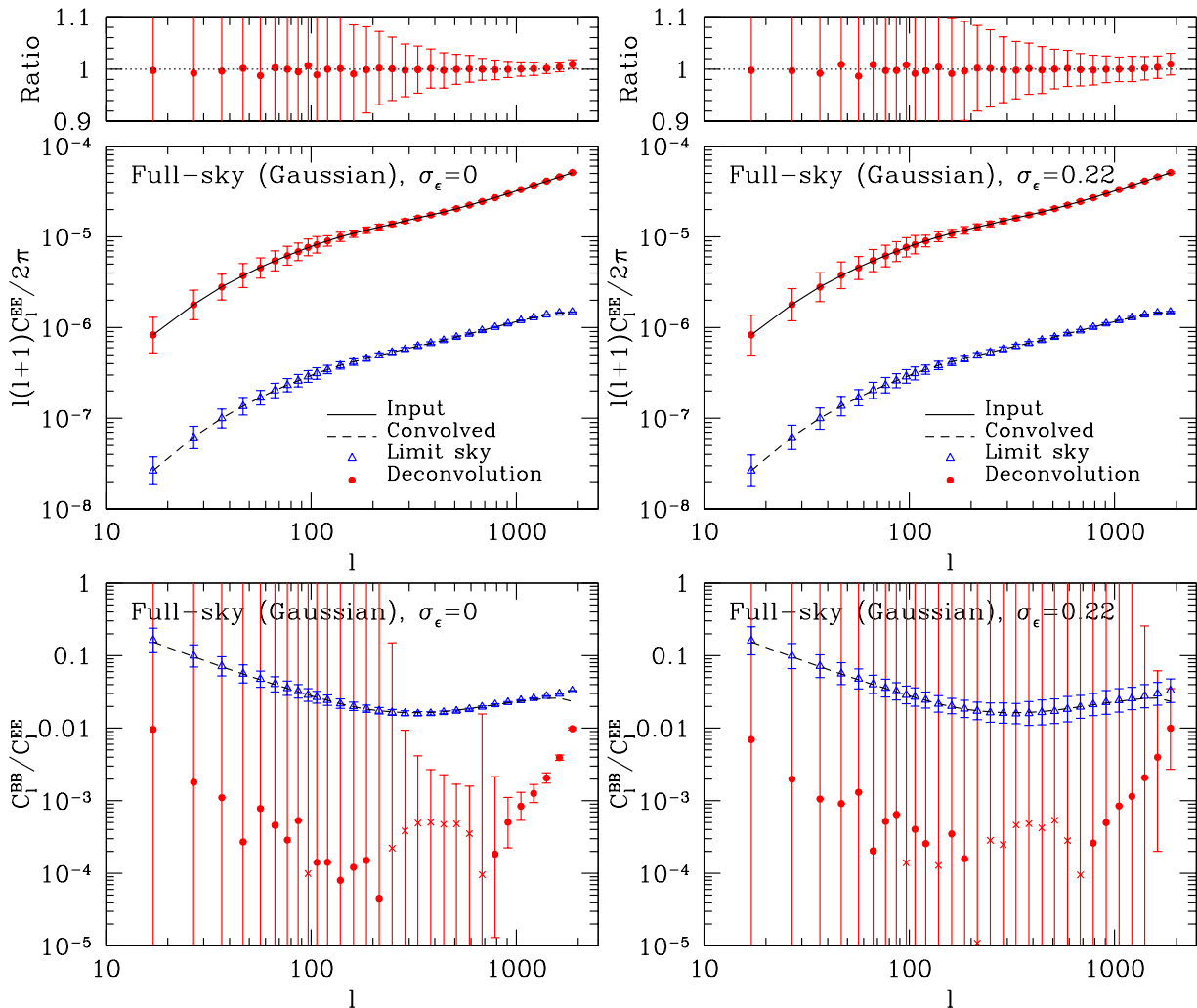


Figure 3. Similar to Fig. 2 but for the Gaussian simulations in full-sky approach using 1000 realizations. Again the method developed in Sec. 2.1 reconstruct the E -mode power spectrum at a sub-percent level. The systematic error in the reconstruction is much smaller than the expected statistical errors for a survey of 2000 sq. deg. coverage, both with (left-panel) and without (right panel) the intrinsic shape noise.

shear power spectrum resides in the modes around $\ell \simeq 1000$ in the presence of the shot noise, Takada & Jain (2009) showed that even a factor 2 increase in the power spectrum errors at the multipoles degrades accuracies of cosmological parameters only by 10-20%. Therefore, the correlated errors due to the survey geometry effect have an insignificant impact on parameter estimation.

5 SUMMARY AND DISCUSSION

We develop a pseudo-spectrum method for reconstructing the cosmic shear power spectra from actual lensing data. The observed shear field is limited to be a finite patch of sky and furthermore roughly 25% of the survey area is masked due to bright stars. We apply for the first time the pseudo-spectrum technique developed in CMB studies to the lensing field and show that our method successfully recovers the shear spectra over a wide range of multipoles from 100 to 10^4 in both full- and flat-sky approaches.

We test the flat-sky method using ray-tracing simulations assuming a square-shaped survey region. The 25% fraction of the total area is masked by realistic configurations for a ground-based survey: circular shapes for bright stars; rectangular shapes for bright star spikes; zero padding in one direction for bad pixels. We show that both the full- and flat-sky methods reconstruct the input E -mode power spectrum in sub-percent accuracy and the residuals are much smaller than the statistical errors of a power spectrum measurement for a survey of 2000 square degree coverage. The residual B -mode power spectrum from the E/B -mode mixing due to the imperfect correction of survey geometry is also suppressed below a percent of the E -mode power spectrum. Our method offers a new means of measuring the cosmic shear correlations and separating the E/B modes from an actual survey data.

Although the pseudo-spectrum technique is promising, our method still yields sub-percent residual of B -mode in the reconstructed power spectra. To further suppress the B -mode spectrum, one has to remove “ambigu-

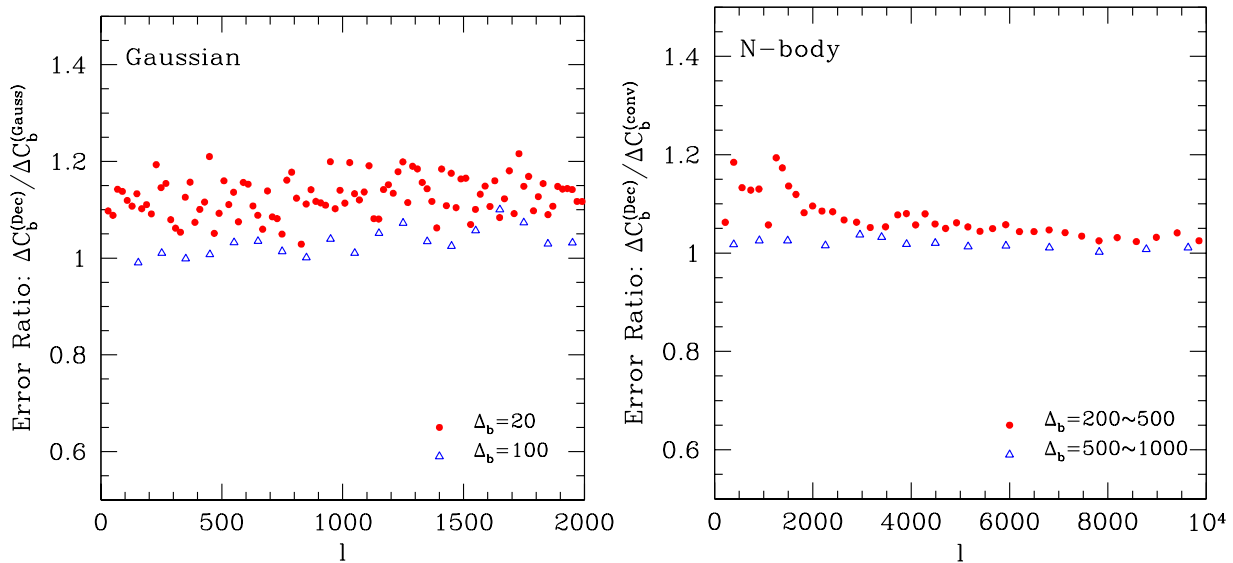


Figure 4. *Left panel:* Error increment of the reconstructed shear power spectrum due to the effects of the finite sky area and the mask. The errors are measured from 1000 realizations of the full-sky Gaussian simulations and then compared with the Gaussian error expectation (Eq.[51]). The survey geometry effect increases the power spectrum errors, but it becomes insignificant at a wider bin width $\Delta l = 100$, about factor 10 wider than the fundamental mode of the 2000 sq. deg. survey area, $l_f \simeq 8$. *Right panel:* Similar to the left panel but for the full simulations in a flat approximation. The error of the reconstructed power is compared with that of the unmasked convergence power of the ray-tracing simulations including the non-Gaussian errors. Again the mask effect increases the errors, which is suppressed at a wider bin width. Note that the non-Gaussian errors do not depend on the bin width.

ous mode” that is inevitably generated in a finite patch of sky (Bunn et al. 2003). The ambiguous mode satisfies both the E -mode (rotation-free) and the B -mode conditions (divergence-free) and thus contaminates E/B -mode spectrum reconstructed using the simple pseudo-spectrum method that we adopt. To eliminate such contamination, Bunn et al. (2003) introduces pure E/B modes that is orthogonal to the ambiguous modes. Pure pseudo C_l estimator and its optimization technique of sky apodization have been developed (Smith 2006; Smith & Zaldarriaga 2007; Grain, Tristram & Stompor 2009; Kim & Naselsky 2010). This technique can be straightforwardly applied to the lensing case.

In this paper we assume that masked regions are uncorrelated with the cosmological shear field. In reality the regions with large shear is preferentially masked: in a region of massive clusters, we cannot obtain a fair sample of background galaxies in the central region due to the dense concentration of member galaxies, where the shearing effect on background galaxies are greater. Masking such a crowded region may bias the power spectrum measurement. This contaminating effect can be estimated by combining ray-tracing simulations with halo catalogs in the underlying N -body simulations. This is our future project, and will be presented elsewhere.

We deeply appreciate Masanori Sato for kindly providing ray-tracing simulation data. We also thank an anonymous referee for careful reading and providing useful comments. C.H. acknowledges support from a Japan Society for Promotion of Science (JSPS) fellowship. This work is in part supported in part by JSPS Core-to-Core Program “International Research Network for Dark Energy”, by Grant-in-

Aid for Scientific Research from the JSPS Promotion of Science (18072001,21740202), by Grant-in-Aid for Scientific Research on Priority Areas No. 467 “Probing the Dark Energy through an Extremely Wide & Deep Survey with Subaru Telescope”, and by World Premier International Research Center Initiative (WPI Initiative), MEXT, Japan.

REFERENCES

- Bacon, D. J., Refregier, A. R., Ellis, R. S., 2000, MNRAS, 318, 625
- Bartelmann, M., & Schneider, P., 2001, Phys. Rep., 340, 294
- Brown, M. L., Taylor, A. N., Bacon, D. J., Gray, M. E., Dye, S., Meisenheimer, K., Wolf, C., 2003, MNRAS, 341, 100
- Brown, M. L., Castro, P. G., Taylor, A. N., 2005, MNRAS, 360, 1262
- Bunn, E. F., 2002, Phys. Rev. D, 65, 043003
- Bunn, E. F., Zaldarriaga, M., Tegmark, M., de Oliveira-Costa A., 2003, Phys. Rev. D, 67, 023501
- Cooray, A., Hu, W., 2001, ApJ, 554, 56
- Crittenden, R. G., Natarajan, P., Pen, U.-L., Theuns, T., 2002, ApJ, 568, 20
- Dahlen, F. A., Tromp, J., 1998, Theoretical Global Seismology. Princeton Univ. Press, Princeton, NJ
- Fu, L., et al., 2008, A&A, 479, 9
- Górski, K. M. et al., 2005, ApJ, 622, 759
- Grain, J., Tristram, M., Stompor, R., 2009, Phys. Rev. D, 79, 123515
- Hamana, T., Mellier, Y. 2001, MNRAS, 327, 169
- Hamana, T., et al., 2003, ApJ, 597, 98

- Hoekstra, H., Jain, B., 2008, *Ann. Rev. Nucl. Part. Sci.*, 58, 99
- Hu, W., White, M., 2001, *ApJ*, 554, 67
- Ichiki, K., Takada, M., Takahashi, T., 2009, *Phys. Rev. D*, 79, 023520
- Jain, B., Seljak, U., White, S., 2000, *ApJ*, 530, 547
- Joachimi, B., Schneider, P., Efler, T., 2008, *A&A*, 477, 43
- Kaiser, N., Wilson, G., Luppino, G. A., 2000, preprint (arXiv:astro-ph/0003338)
- Kim, J., Naselsky, P., 2010, preprint (arXiv:1003.2911)
- Kogut, A., et al., 2003, *ApJS*, 148, 161
- Limber, D. N., 1954, *ApJL*, 119, 655
- Miyazaki, S., et al., 2006, *SPIE*, 6269, 9
- Pielorz, J., Rödiger, J., Tereno, I., Schneider, P., 2009, preprint (arXiv:0907.1524)
- Refregier, A., et al. 2010, preprint (arXiv:1001.0061)
- Sato, M., Hamana, T., Takahashi, R., Takada, M., Yoshida, N., Matsubara, T., Sugiyama, N., 2009, *ApJ*, 701, 945
- Schneider, P., Van Waerbeke, L., Jain, B., Kruse, G., 1998, *MNRAS*, 296, 873
- Schneider, P., Van Waerbeke, L., Kilbinger, M., Mellier, Y., 2002, *A&A*, 396, 1
- Schneider, P., Eifler, T., Krause, E., 2010, preprint (arXiv:1002.2136)
- Schrabback, T., et al., 2010, *A&A*, 516, 63
- Seljak, U., 1998, *ApJ*, 506, 64
- Semboloni, E., et al., 2007, *MNRAS*, 375, L6
- Smith, K. M., 2006, *Phys. Rev. D*, 74, 083002
- Smith, K. M., Zaldarriaga, M., 2007, *Phys. Rev. D*, 76, 043001
- Spergel, D. N., et al., 2007, *ApJS*, 170, 377
- Springel, V., 2005, *MNRAS*, 364, 1105
- Takada, M., Bridle, S., 2007, *New J. Phys.*, 9, 446
- Takada, M., Jain, B., 2009, *MNRAS*, 395, 2065
- Van Waerbeke, L., et al. 2000, *A&A*, 358, 30
- Wandelt, B. D., Hivon, E., Gorski, K. M., 2001, *Phys. Rev. D*, 64, 083003
- Wittman, D. M., Tyson, J. A., Kirkman, D., Dell'Antonio, I., Bernstein, G., 2000, *Nature*, 405, 143